

Mapping a depinning transition to polynuclear growth

G.J. Szabó^{1,2} and M.J. Alava¹

¹*Helsinki University of Technology, Laboratory of Physics, P.O.Box 1100, FIN-02015 HUT, Finland*

²*Technical University of Budapest, Department of Theoretical Physics, H-1111 Hungary*

We develop a phenomenological mapping between submonolayer polynuclear growth (PNG) and the interface dynamics at and below the depinning transition in the Kardar–Parisi–Zhang equation for a negative non-linearity λ . This is possible since the phase transition is of first-order, with no diverging correlation length as the transition is approached from below. The morphology of the still-active and pinned configurations and the interface velocity are compared to the PNG picture. The interface mean height scales as $\text{erf}(t)$.

PACS # 05.70.Np, 75.50.Lk, 68.35.Ct, 64.60.Ht

I. INTRODUCTION

The dynamics of driven manifolds in random media presents many examples of non-equilibrium phase transitions. The interest lies often in how an object interacts with a quenched disorder environment. If the driving force is small enough and the temperature zero, the manifold, e.g. a domain wall in a magnet, or an interface between two phases, can get pinned. This means, quite simply, that its velocity becomes zero. Therefore one can discuss the physics in terms of an order parameter (velocity) and a control parameter (external force). At and close to the critical force value F_c the driven interface can develop critical correlations due to the frustration that arises from the competition between, typically, elastic forces and the randomness of the medium [1–6].

An example is provided by the quenched Kardar–Parisi–Zhang (QKPZ) equation,

$$\frac{\partial h(\mathbf{x}, t)}{\partial t} = \nu \nabla^2 h + \frac{\lambda}{2} (\nabla h)^2 + F + \eta(\mathbf{x}, h). \quad (1)$$

where h is the interface height, ν a surface tension, λ the strength of the nonlinearity characterizing the KPZ class [7], F a driving force, and η is the quenched noise. If λ is positive and stays finite in the limit $F \rightarrow F_c^+$, the depinning phase transition in 1+1 dimensions can be mapped to directed percolation (DP) via a geometrical construction. In this way one can compute the critical exponents through the knowledge concerning the DP exponents, and the particular model where this is explicitly possible has been coined ‘directed percolation depinning’ one for obvious reasons [8–10].

If λ is negative, however, the character of the transition changes completely. Fig. 1 shows an example of an interface at $F \sim F_c$. The depinning in this case was investigated by Jeong, Kahng, and Kim [11], who showed that the transition becomes of a *first-order* kind and that this persists even in the presence of finite tilts below a critical m_c . The aim of this article is to use a new geometrical construction to discuss the morphology in the case depicted in Fig. 1, similarly in spirit to the DPD-mapping of the $\lambda > 0$ -case.

The essential physics in the $\lambda < 0$ QKPZ class, at and below F_c arises from “facet formation”, the fact that the

slopes of the triangular mounds are just dependent on the parameters of the equation, and from “valley formation”. A look at Fig. 1 where the interface is shown at various times t_i implies that it is these two mechanisms that are responsible for the final shape of an interface that gets pinned. In this article we map the two-dimensional growth of the QPKZ interfaces to a one-dimensional submonolayer polynuclear growth model (PNG) [12] based on this picture of a statistically constant growth velocity of the facets, and random pinning events on the roughly speaking planar areas of growth. This implies that one can understand the pinning of an interface in a quenched environment by considering a model with ‘thermal noise’, only. The reason why this is possible is the first-order character of the transition: there is no diverging correlation length, and therefore the physics of the depinning can be understood based on a local picture of events. Notice that the PNG in the multilayer version is actually in the thermal KPZ-class, and that the relation in our case between a growth model and the PNG is indirect.

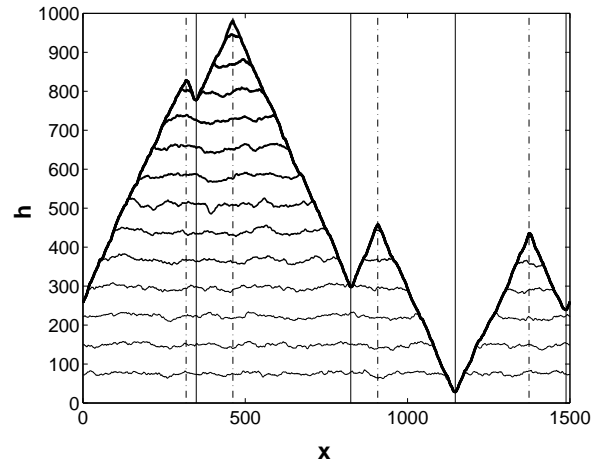


FIG. 1. Temporal evolution of a QKPZ interface at an external driving of $F = 14.5$. The snapshots have been taken every 1000th time step. The vertical slicing lines designate the positions of “valleys” and “peaks” located by the algorithm described in the text.

Section two of this paper introduces the actual numerical QKPZ model and the relevant parameters. In Section three, we discuss in detail the mapping between the QKPZ and the PNG models including a measurement of the model parameters for use in the PNG model. We also discuss the relevant parts of the PNG literature. In Section four the free parameters (growth velocity, pinning probability per unit time) are discussed and computed, and a basic comparison of the QKPZ interfaces with those that come from the PNG representation is presented. Section five finishes the paper with a discussion.

II. NUMERICS

The model we focus on is a $1 + 1$ dimensional QKPZ system with the spatial coordinate x and time t discretized, while the interface height h is a continuous number. We use periodic boundary conditions with flat initial configuration. The forthcoming results have been obtained from systems in which the equation coefficients are invariably $\nu = 10$, $\lambda = -4$, and $g = 20$.

The system is updated simultaneously for all lattice sites in every time step according to the finite differences version of the governing equation (1) with $\Delta t = 0.01$:

$$\begin{aligned} f_i(t) &= \nu[h_{i+1}(t) + h_{i-1}(t) - 2h_i(t)] + \\ &+ \frac{\lambda}{8}[h_{i+1}(t) - h_{i-1}(t)]^2 + F + g\eta_i([h_i(t)]) \\ h_i(t + \Delta t) &= \begin{cases} h_i(t) + f_i\Delta t & \text{if } f_i(t) > 0 \\ h_i(t) & \text{otherwise} \end{cases} \end{aligned} \quad (2)$$

The value of the noise term η_i at integer positions of the height field denoted by $[\cdot]$ is chosen randomly from the interval $[-1; 1]$ with a uniform distribution and is unchanged in time. The choice of the noise term is meant to mimic the simulation carried out in [11]. Nevertheless, the particular form of η_i has a mere quantitative influence on some measurables such as the critical driving force F_c ; the qualitative behavior of the systems have been checked to yield consistent results independently of the various options for the representation of η_i .

We study the morphology of slightly subcritical interfaces with the mapping to the PNG model in mind. To this end we identify the macroscopic facets along the interface locating the “valleys” and “peaks” in the entirely evolved and stopped systems.

The algorithm to find the extrema is composed as follows. As a first step the pinned interface is scanned for all of the local minima and maxima positions. Subsequently after that, the pair of adjacent minimum/maximum with the smallest distance to each other is removed and this step repeated until the distance between the two closest extremal positions is no more than a specific parameter. Applying this procedure we eliminate the noise-like small height fluctuations of the interface. The resolution of the

facets depends on the actual choice of the smallest distance parameter and we use a few lattice units for that.

III. MAPPING TO THE POLYNUCLEAR GROWTH MODEL

A. The interface growth in one dimension

Following the time evolution of some interface configurations like the one in Fig. 1, it suggests itself that the pinning events resulting in the valleys of the final morphology take place in a seemingly random way on the growing terraces. The interface is observed to propagate with a uniform average vertical velocity at the plateaus of the facets, in other words, the height of the separated terraces of the interface is on the average on the same level at all times. The straight sides of the facets mean that the horizontal distance between the end points of neighboring facets at the level of propagation grows in a linear fashion with time, following to first order from a balance between the nonlinearity and the driving force in Eq. (1).

If we consider the h axis of Fig. 1 as time and the sides of the final interface facets as phase boundaries in this model, we can outline a picture of a model mapping as follows. We define a one dimensional lattice of cells on the grounds of the PNG model with two-state filling possibilities: a site is either occupied by a particle or empty, with an initially empty configuration. During the simultaneous updating steps of the lattice, a seed particle may be deposited to any of the empty cells with a certain probability in every time step. The actual deposition probability and place may depend on various factors which will be discussed later.

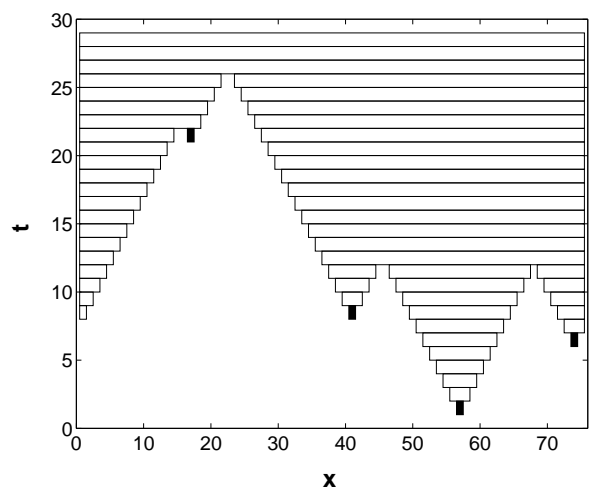


FIG. 2. Time evolution of PNG islands with the seeds filled black. The mapping is performed for the interface configuration depicted in Fig. 1 with a system size rescaling factor of $\Lambda = 0.05$.

Deposition of seeds creates growing islands with one particle added per time step at both ends according to the formal rule of

$$s_i(t+1) = \begin{cases} 1 & \text{if } s_{i-1}(t) = 1 \text{ or } s_{i+1}(t) = 1 \\ s_i(t) & \text{otherwise} \end{cases} \quad (3)$$

$s_i(t)$ denotes the filling state of the cell i at time t . An occupied site is marked by 1 while an empty one is marked by 0. In other words (3) means that a cell gets filled if either of its neighbors is already filled. The system has periodic boundary conditions so $s_{i-1} = s_L$ for $i = 1$ and $s_{i+1} = s_1$ for $i = L$. L is the lattice size and the indices run from 1 to L .

It is obvious that if we associate the empty cells in this model with the still-growing parts of the interface and the filled cells with the uncovered regions, the time evolution of the system would give a very similar picture to the final configuration of Fig. 1, if the way the seeds are deposited is chosen the right way. An example of the mapping is demonstrated by Fig. 2.

Fig. 3 suggests that the probability the first seed is introduced at a given time should decay exponentially in time, which is the earmark of a geometric process. This means that the probability of a seed deposition (the creation of the first pinned site) has a constant probability per each time step. If this is true, then the growth closely resembles the submonolayer polynuclear growth model (PNG), or the Kolmogorov–Avrami–Johnson–Mehl (KAJM) model [15–17]. (The PNG model is originally defined so that the growth itself takes place in many layers atop each other.)

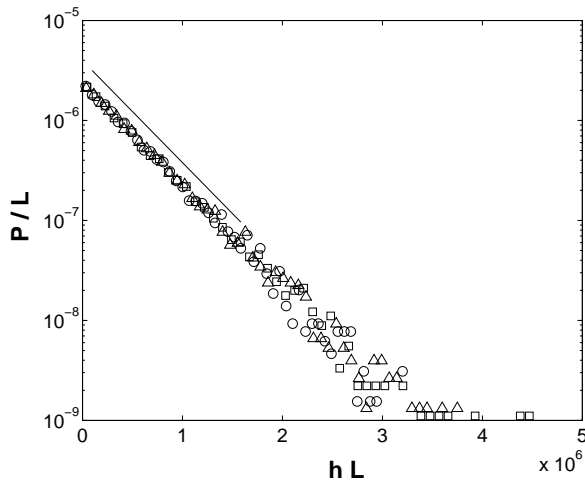


FIG. 3. The probability distribution P of the first pinning height h in the KPZ system, rescaled by the system size of 500, 1000, and 2500 for \circ , \triangle , and \square , respectively. The driving force is $F = 14.8$. The averaging is done for 10000 interface configurations in each case. The rescaled distribution is found to decay exponentially with an associated exponent of $b \approx 2.35 \cdot 10^{-6}$ in the range of the parallel line shown in the figure.

Another crucial question is: how is the pinning probability or the nucleation probability in the PNG picture dependent on F ? Fig. 4 illustrates the progress of two quantities close to the estimated F_c . Both the average number of pinning events and the average height (time) of the first pinning event scale roughly as power laws with $|F - F_c|$. Since the depinning transition is of first order, it is not a priori obvious how these quantities should behave as $F \rightarrow F_c^-$. The most natural guess is that the pinning probability per site per time-step goes to zero continuously, which would indicate that $h(F)$ and $N(F)$, as depicted in Fig. 4, should approach infinity and zero, respectively with cut-offs imposed by the maximum time the interfaces are followed, and the system size, respectively.

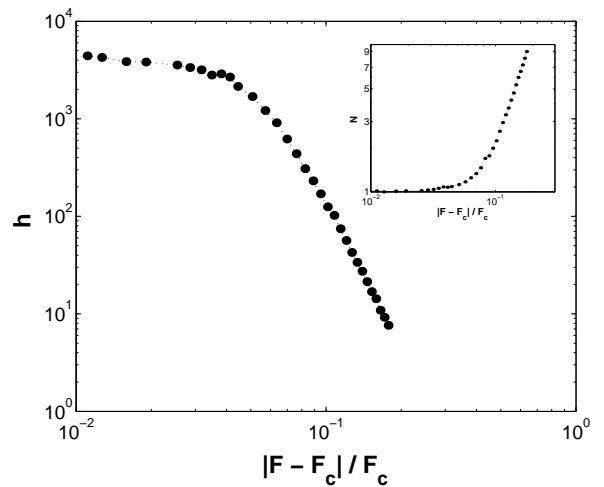


FIG. 4. The first pinning height h as function of the driving force $|F - F_c|/F_c$ for a system of 500 lattice units. The saturation is caused by limitations imposed on the maximum time configurations are allowed to evolve because of practical reasons. The inset shows the number of pinnings taking place.

B. Interface morphology

The valleys and peaks are identified like described in Section II. The side gradients of the facets are measured on both sides and are displayed for various system configurations in Table I. The height and position of the pinning events are also determined and recorded. F is chosen so that the system develops only a limited number of facets; this way, the uncertainty of facet identification and measurement stays under control. On the other hand, we are mainly interested in the behavior when $F \lesssim F_c$. We do not determine F_c with very great accuracy; good estimates can be found in [11].

According to Table I, the facet side gradients are independent of system size for a given F . Additionally, the left and right hand side slopes are the same as well, as expected in the absence of a global tilt. In contrast to this, the number of pinning events taking place in the

systems is subject to finite size scaling. The error values associated with the averages are apparently large (30–40%).

C. PNG theory

For the next section where the growth statistics are compared with the one-dimensional picture some results are needed about the interesting quantities. In the ordinary KAJM theory islands are nucleated on a line randomly, with a rate γ and grow at a constant velocity. To map to the KPZ case one needs a function that relates that velocity to the KPZ mound slopes as discussed below. If one has $N(t)$ nucleated islands (here pinned parts of the interface) then the fraction of uncovered space (here growing fraction of interface) $S(t)$ satisfies the rate equation $dS/dt = -N$ with a proportionality factor chosen as unity. It is easy to understand that in a large system the temporal fluctuations of the slopes of the growing KPZ interface average out, to an average growth velocity in the KAJM picture. This holds if the slopes do not depend on e.g. the size of the terrace they are adjacent to which seems trivially true. Then the only factor that needs to be checked is whether the nucleation events happen randomly, with a constant density as in the simple KAJM as discussed above.

In the one-dimensional picture, one can proceed by defining size distributions for the islands, for the gaps between the island, and finally the density of islands that contain a fixed number of seeds, n . The last one implies that such islands result from the coalescence of n single-seed islands. Such distributions describe exactly the KPZ interface in the KAJM language (assuming that the mapping to PNG/KAJM works out). The last of these distributions is hard to compute since it involves a solution of a Smoluchowski-like equation for the densities for different n . We quote here some of the appropriate results from [13,14]. First, the island number density,

$$N(t) \sim te^{-t^2}, \quad (4)$$

corresponds to the number of valleys in the KPZ picture (as, also, a function of average interface height, $N(h)$). Second, the uncovered fraction gives directly the interface velocity after a proper normalization, and reads

$$S(t) = e^{-t^2/2}, \quad (5)$$

implying a fast decay of the growth.

IV. COMPARISON OF THE PNG PICTURE WITH THE KPZ MODEL

Following the considerations above, let us denote the probability of a seed deposition per lattice unit in the PNG model Π for every time step. Π should be tuned

appropriately so that the average number of seed depositions equals the average number of pinning events or valleys in the KPZ system. This is the only parameter that affects the “morphology” in this system, while another one, an artificial “side gradient” μ has also to be introduced to transform the time scale of the PNG model to length scale in the KPZ counterpart.

Notice that the virtual valleys and summits from the PNG model after the scale transformation are not rounded. The presence of the surface tension term in the KPZ equation counteracts such sharp corners, though. Still, if the strength of the surface tension coefficient ν is sufficiently small, the resulting interface is very similar to the one obtained from the PNG model.

To achieve proper quantitative predictions and match between the KPZ morphology statistics and the PNG picture, we need to tune Π and μ so that measuring the first pinning height (seed deposition time) distribution, we end up with the same decay exponents. We relate the general height in the KPZ model h_{KPZ} to time in the PNG system t_{PNG} as $h_{KPZ} = \mu t_{PNG}$. The probability of the first seed deposition follows a geometric process:

$$\begin{aligned} P(t_{PNG} = \tau) &= P(h_{KPZ}/\mu = \tau) = (1-p)^{\tau-1}p = \\ &= (1-p)^{\chi_{KPZ}/\mu-1}p \\ \log P(t_{PNG} = \tau) &= \log \frac{p}{1-p} + \frac{\log(1-p)}{\mu} \chi_{KPZ}, \end{aligned} \quad (6)$$

if p denotes the seed depositing probability for the entire length of the PNG system, that is, $p = \Pi L_{PNG}$. χ_{KPZ} is the first pinning height (the altitude of the lowest valley) in the corresponding KPZ system. Comparing Fig. 3 to Eq. (6) we find that the assumption of $p = \text{const.}$ is valid.

The experimental value of the probability decay exponent β in the KPZ system should thus equal $\log(1-p)/\mu$ expressed by the PNG parameters. The Taylor series expansion of the later results in $p = -\beta\mu \ln 10$ up to first order.

If the horizontal scale transformation between the KPZ and PNG systems is given by $L_{PNG} = \Lambda L_{KPZ}$, then μ can simply be calculated from the measured facet side gradients in the KPZ system, summarized in Table I. Then if s denotes the empirical value of the side slope, $\mu = s/\Lambda$. According to these, the normalized seed deposition probability Π is obtained as

$$\Pi = -\frac{\beta s \ln 10}{\Lambda L_{PNG}}. \quad (7)$$

The discussion above assumed that the parameter matching is performed between two particular lattices of specific features, most importantly the number of cells in the systems. Considering the data collapse of Fig. 3, though, an additional relation for β emerges instantly: $\beta \sim L_{KPZ}$, provided that the equation parameters (ν , λ , F , g) are otherwise fixed. Since s does not explicitly depend on L_{KPZ} , and if $\beta = bL_{KPZ}$,

$$\Pi = -\frac{bL_{KPZ}s \ln 10}{\Lambda(\Lambda L_{KPZ})} = -\frac{bs \ln 10}{\Lambda^2}. \quad (8)$$

A further consequence of the fact that $P \sim \Phi(hL_{KPZ})$ for the first pinning probability with a suitable scaling function Φ , is that the general pinning probability per time unit in propagating fronts of a QKPZ system is *linearly proportional* to the integrated local interface velocity, $v(x, t)$,

$$P_{pinning}(t) \sim \int v(x, t) dx. \quad (9)$$

Using the parameters above it is possible to completely recover the exact scaling law of the first pinning event in a system conforming to the KPZ equation. It may still be uncertain, though, whether the subsequent pinning events follow the same governing rules as the first one, in particular the assumption that the seed creation probability is linearly proportional to the island length.

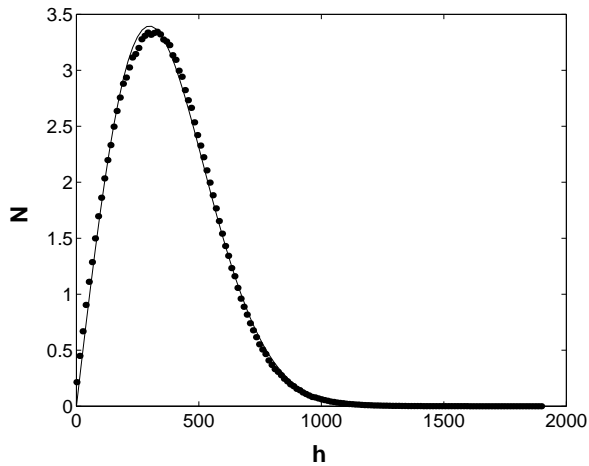


FIG. 5. The “island number” distribution $N(h)$ calculated for a KPZ system according to the text. Since the interface propagation velocity is constant, h can be appropriately rescaled so as to yield time in a PNG system. The system size is 2500, while the driving force is $F = 14.5$. The number of averaging iterations is 10000. The theoretical function of $N(h) = A h \exp(-B h^2)$ is fitted to the empirical data points minimizing the quadratic error and giving the results of $A = 5.84 \cdot 10^{-3}$ and $B = 2.33 \cdot 10^{-6}$. The slight shift of the distribution maximum may come from the fact that an initially flat interface cannot get pinned before the necessary fluctuations develop. On the other hand, the omission of very small facets can have an unwanted effect on the data as well.

In order to verify this assumption, we perform an “island counting” measurement on the KPZ ensembles with the ultimate goal of deriving the number of islands versus time statistics, $N(t)$. Islands are interpreted in a straightforward way: an island is created in the associated PNG system whenever a pinning event occurs, and two islands adjoin to form one at the facet summits of

the interface, reducing the actual number of islands by one. An illustration of the island construction is shown in Fig. 2. This thought experiment leaves us with a way to construct the associated island number distribution in function of the time (height) in the KPZ model. The $N(t)$ function for the individual samples is naturally composed of step functions taking on the appropriate integer constants between the respective time (height) intervals. The PNG and KPZ behaviors are in good correspondence, which is a strong evidence for the validity of our assumptions. The experimental relation for $N(t)$ calculated in KPZ systems is shown in Fig. 5 together with the curve fitted based on the KAJM result, Eq. (4).

An associated quantity is the average height of the interface in time, which can be measured in a very simple way in contrast to $N(t)$ mentioned in the preceding paragraphs. Let $S(t)$ denote the uncovered fraction of a PNG system, Eq. (5). Thus,

$$\langle h_{KPZ}(t) \rangle = \frac{1}{L} \int_0^L h_{KPZ}(x, t) dx = \int_0^t S(\tau) d\tau. \quad (10)$$

Fig. 6 shows the empirical relation found for $\langle h_{KPZ}(t) \rangle$ and the adequately scaled error function for a given interface evolution. Again, the theory proves to be consistent with our experimental data to a high degree of confidence.

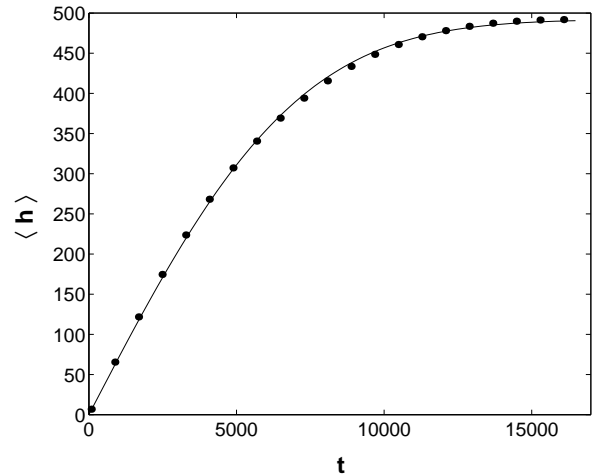


FIG. 6. The averaged interface height $\langle h \rangle$ versus time t , the latter measured in lattice updating steps. A system of 10000 lattice units is used. The guide line is obtained from fitting $\sqrt{\pi/4} A \operatorname{erf}(Bt)$ in a least-squares sense with $A = 555$ and $B = 1.27 \cdot 10^{-4}$.

V. SUMMARY

In this paper we point out a mapping between interfaces in two-dimensional systems, described by the negative- λ quenched Kardar–Parisi–Zhang equation and a one-dimensional island growth model. An investigation of KPZ interfaces reveals that pinning processes give rise

to a morphology with valleys and facets that are formed. The facets are found to have straight edges with vanishing deviations on a macroscopic scale, as well as sharp corners. This establishes a connection with the PNG or KAJM model. The correspondence is supported by evidence based on comparing statistical quantities in both ensembles. Considering the KPZ model from this point of view, it can be stated that pinning events are the manifestation of a local nucleation process that is uncorrelated both in time and space. The pinning probability for an interface segment which advances covering an area of dA only depends on dA in an exponentially decaying fashion.

The work presented here gives a geometric description of the $\lambda < 0$ -depinning transition, in analogy to the directed percolation depinning-picture of the opposite, $\lambda > 0$ -case. There it is possible to extend the correspondence of the geometrical construction and the pinned interfaces at F_c to higher dimensions [20]. In our case this still awaits further work, but one should note that the KAJM model of island growth becomes much more difficult to handle, analytically, in $d > 1$ [18,19].

This work has been supported by the Academy of Finland's Centre of Excellence Programme.

-
- [1] A.-L. Barabási and H. E. Stanley, *Fractal concepts in surface growth*, (Cambridge University Press, Cambridge, U.K., 1995).
[2] T. Halpin-Healy and Y.-C. Zhang, Phys. Rep. **254**, 215 (1995).

- [3] M. Kardar, Phys. Rep. **301**, 85 (1998).
[4] D. Fisher, Phys. Rep. **301**, 113 (1998).
[5] L.-H. Tang, M. Kardar, and D. Dhar, Phys. Rev. Lett. **74**, 920 (1995).
[6] K. Sneppen, Phys. Rev. Lett. **69**, 3539 (1992).
[7] M. Kardar, G. Parisi, and Y.-C. Zhang, Phys. Rev. Lett. **56**, 889 (1986).
[8] L. A. N. Amaral, A.-L. Barabási, S. V. Buldyrev, S. Havlin, and H. E. Stanley, Phys. Rev. Lett. **72**, 641 (1994).
[9] L.-H. Tang and H. Leschhorn, Phys. Rev. A **45**, R8309 (1992) and S. V. Buldyrev, A.-L. Barabási, F. Caserta, S. Havlin, H. E. Stanley, and T. Vicsek, Phys. Rev. A **45**, R8313 (1992).
[10] F. Family and T. Vicsek, J. Phys. A **18** L75 (1985).
[11] H. Jeong, B. Kahng, and D. Kim, Phys. Rev. E **59**, 1570 (1999).
[12] F. C. Frank, J. Cryst. Growth **22**, 233 (1974), and J. Kertész and D. E. Wolf, Phys. Rev. Lett. **62**, 2571 (1989).
[13] E. Ben-Naim and P. L. Krapivsky, Phys. Rev. E **54**, 3562 (1996).
[14] E. Ben-Naim, A. R. Bishop, I. Daruka, and P. L. Krapivsky, J. Phys. A **31**, 5001 (1998).
[15] A. N. Kolmogorov, Izv. Akad. Nauk SSSR, Ser. Fiz. **1**, 335 (1937) [Bull. Acad. Sci. USSR, Phys. Ser. **1**, 355 (1937)].
[16] M. Avrami, J. Chem. Phys. **7**, 1103 (1939); **8**, 212 (1940); **9**, 177 (1941).
[17] W. A. Johnson and P. A. Mehl, Trans. AIMME **135**, 416 (1939).
[18] K. Sekimoto, Int. J. Mod. Phys. **B 5**, 1843 (1991).
[19] K. Sekimoto, Physica A **135**, 328 (1986).
[20] S. Buldyrev, S. Havlin, J. Kertész, R. Sadr-Lahijany, A. Shehter, and H. E. Stanley, Phys. Rev. E **52**, 373 (1995).

F	Size	Pinnings	Gradient left	Gradient right
13.5	500	10.63 ± 3.02	1.483 ± 0.087	1.484 ± 0.086
	1000	10.26 ± 2.07	1.483 ± 0.066	1.484 ± 0.067
	2500	9.93 ± 1.24	1.482 ± 0.039	1.482 ± 0.040
14.0	500	5.80 ± 2.13	1.652 ± 0.085	1.654 ± 0.085
	1000	5.65 ± 1.46	1.652 ± 0.069	1.653 ± 0.066
	2500	5.53 ± 0.89	1.651 ± 0.041	1.650 ± 0.041
14.5	500	3.22 ± 1.42	1.798 ± 0.093	1.797 ± 0.095
	1000	2.85 ± 1.02	1.802 ± 0.068	1.802 ± 0.076
	2500	2.79 ± 0.63	1.800 ± 0.041	1.800 ± 0.042
14.8	500	2.49 ± 0.94	1.869 ± 0.085	1.869 ± 0.093
	1000	1.86 ± 0.80	1.878 ± 0.073	1.879 ± 0.069
	2500	1.74 ± 0.50	1.879 ± 0.039	1.877 ± 0.039

TABLE I. Comparison table of interface morphology for close-to-critical systems with different external driving forces; $F_c \approx 15$. The “Pinnings” column contains the average number of valleys found in the systems, normalized to 1000 lattice units. The “Gradient left” and “Gradient right” columns show the average slope on the left hand side and right hand side of the facets, respectively. The number of interface samples averaged is 10000 in each of the cases. The errors are measured by the standard deviation of the respective quantities.